Stochastic coordination of multiple actuators reduces latency and improves chemotactic response in bacteria

Michael W. Sneddon[a,b], William Pontius[b,c], and Thierry Emonet[a,b,c,1]

[a]Interdepartmental Program in Computational Biology and Bioinformatics, [b]Department of Molecular, Cellular and Developmental Biology, and [c]Department of Physics, Yale University, New Haven, CT 06520

Edited by Howard C. Berg, Harvard University, Cambridge, MA, and approved November 11, 2011 (received for review August 19, 2011)

Individual neuronal, signal transduction, and regulatory pathways often control multiple stochastic downstream actuators, which raises the question of how coordinated response to a single input can be achieved when individual actuators fluctuate independently. In *Escherichia coli*, the bacterial chemotaxis pathway controls the activity of multiple flagellar motors to generate the run-and-tumble motion of the cell. High-resolution microscopy experiments have identified the key conformational changes adopted by individual flagella during this process. By incorporating these observations into a stochastic model of the flagellar bundle, we demonstrate that the presence of multiple motors imposes a trade-off on chemotactic performance. Multiple motors reduce the latency of the response below the time scale of the stochastic switching of a single motor, which improves performance on steep gradients of attractants. However, the uncoordinated switching of multiple motors interrupts and shortens cell runs, which thereby reduces signal detection and performance on shallow gradients. Remarkably, when slow fluctuations generated by the adaptation mechanism of the chemotaxis system are incorporated in the model at levels measured in experiments, the chemotactic sensitivity and performance in shallow gradients is partially restored with marginal effects for steep gradients. The noise is beneficial because it simultaneously generates long events in the statistics of individual motors and coordinates the motors to generate a long tail in the run length distribution of the cell. Occasional long runs are known to enhance exploration of random walkers. Here we show that they have the additional benefit of enhancing the sensitivity of the bacterium to very shallow gradients.

Lévy walk | agent-based | motility | search strategy | signal processing

Escherichia coli performs a random walk by controlling the rotational direction of multiple flagellar motors (1). Counterclockwise (CCW) rotation of the motors promotes formation of a coherent flagellar bundle that propels the cell forward. Clockwise (CW) rotation of any single motor causes the corresponding flagellum to change conformation, exit the bundle, and generate a reorientation event called a tumble (2, 3). Through the bacterial chemotaxis pathway, *E. coli* regulates the frequency of tumbles to bias its random walk in favorable directions. The core of the chemotaxis network is a two-component signal transduction system in which binding of an external attractant by clusters of transmembrane chemoreceptors leads to rapid (<1 s) inhibition of the activity of the associated histidine kinase, CheA, thereby depleting the phosphorylated form of CheY (CheY-P), a diffusible response regulator that binds to the base of the motor. Lower levels of CheY-P increase the probability that flagellar motors rotate CCW and, thus, increase the mean duration of runs in response to the attractant. The network adapts to persistent stimuli at a slower time scale (approximately 15 s) by competitive methylation and demethylation of the chemoreceptors by the adaptation enzymes CheR and CheB respectively, returning the chemoreceptors to a sensitive state (4).

Many studies of the *E. coli* chemotaxis system have analyzed how external stimuli are converted into the rotational state of a single motor (5–14). The relevant output for a motile cell, however, is the duration and statistics of runs and tumbles, which result from the integration of multiple flagellar states (2, 3, 7, 10). Although some work has explored the hydrodynamics of the flagellar bundle (15–17) and the physics of motor switching under load (18–21), it remains prohibitively difficult, both theoretically and computationally, to incorporate such information into models designed to study signal processing and motility over long time scales or large populations. Relatively recently, Berg and colleagues used high-resolution fluorescence microscopy (2, 3) to document how a typical tumble event is likely to arise from a single motor switching to CW rotation within the bundle (Fig. 1). These observations laid the foundation for understanding the implications of multiple flagella for bacterial chemotaxis, which so far remain unclear.

Here we build a coarse-grained stochastic model of multiple flagellar motors and flagellar interactions on the basis of the observations of Berg and colleagues (2, 3) and couple it to a model of signal transduction. We then analyze the consequences of multiple flagellar motors on signal processing and motile behavior by performing agent-based simulations of populations of up to 10^5 individual cells.

Results

Conformation Model of Multiple Flagella. We built a stochastic, phenomenological model of flagellar motors, conformations, and interactions that integrates results from multiple experimental observations (2, 3, 8, 22). Individual motors are modeled as stochastic bistable systems (23, 24) in which the transition rates k_+ and k_- to CCW and CW rotation, respectively, are functions of the concentration of CheY-P, Y_p:

$$k_\pm = \omega \cdot \exp\left\{\pm\left[\frac{g_0}{4} - \frac{g_1}{2}\left(\frac{Y_p(t)}{Y_p(t)+K_D}\right)\right]\right\}, \qquad [1]$$

with parameters ω, g_0, g_1, and K_D chosen to fit single motor experimental data (8, 22) (*SI Appendix*, Fig. S1).

Each flagellum is modeled as a three-state system (Fig. 1) with states corresponding to normal, semicoiled, or curly-1 conformations and transitions between states dependent on the rotational state of the motor (2). When rotating CCW, the flagellum adopts the left-handed normal conformation. After a switch to CW and a short delay $d = 0.015$ s arising from propagation of the conformational change through the tip of the flagellum, the flagellum adopts a right-handed semicoiled conformation (2). If CW rota-

Author contributions: M.W.S. and T.E. designed research; M.W.S. and W.P. performed research; M.W.S., W.P., and T.E. analyzed data; and M.W.S., W.P., and T.E. wrote the paper.

The authors declare no conflict of interest.

This article is a PNAS Direct Submission.

[1]To whom correspondence should be addressed. E-mail: thierry.emonet@yale.edu.

This article contains supporting information online at www.pnas.org/lookup/suppl/doi:10.1073/pnas.1113706109/-/DCSupplemental.

tion persists, the semicoiled form gives way to the more stable right-handed curly-1 conformation that wraps around the flagellar bundle with constant rate $\bar{\lambda}^{-1} = 5\ \mathrm{s}^{-1}$. At any point, a switch of the motor back to CCW returns the flagellum from either semicoiled or curly-1 to the normal conformation after a delay d. Let $f_i(t)$ be the conformational state of flagellum $i = 1 \ldots N$ at time t, where N is the number of flagella. Let $m_i(t)$ be the rotational state, CW or CCW, of motor i at time t. Finally, let $T_i^m(t)$ be the cumulative length of time that motor i has been in state $m_i(t)$. Then, the next conformational state of flagellum i after a small time step dt is determined according to the following update rules:

$$f_i(t+dt) = \begin{cases} \text{NORM} & \text{if } m_i(t+dt) = \text{CCW and } T_i^m(t) > d + dt, \\ \text{SEMI} & \text{if } m_i(t+dt) = \text{CW and } d + dt < T_i^m(t) < d + \lambda_i + dt, \\ \text{CURLY} & \text{if } m_i(t+dt) = \text{CW and } T_i^m(t) > d + \lambda_i + dt \\ f_i(t) & \text{otherwise,} \end{cases} \quad [2]$$

where λ_i is sampled for each flagellum i that switches to semicoiled according to an exponential distribution with mean $\bar{\lambda} = 0.2$ s.

As in other modeling studies (10, 13, 14, 25, 26), we consider the state of a cell to be either running or tumbling. For a cell to be running, it is assumed that at least x out of the N flagella must be in the normal conformation to form a coherent bundle. Flagella rotating CW but in the curly-1 conformation can wrap around the main bundle, and the cell can continue a run. However, any flagellum in the semicoiled state generates a tumble. Eqs. **1** and **2** are integrated numerically to obtain trajectories of single cell states (*SI Appendix*).

Analytical expressions for the steady-state statistics of the flagellar motors and cell states as a function of Y_p can be obtained under the simplifying assumption that conformations propagate instantaneously along a flagellum—i.e., $d \approx 0$ (*SI Appendix*). In this case, the probability for a motor to be rotating CW is $P_{\mathrm{CW}} = k_-/(k_+ + k_-)$, and the conditional probability that its flagellum is in the curly-1 conformation is $P_{\mathrm{CURLY|CW}} = \bar{\lambda}^{-1}/(k_+ + \bar{\lambda}^{-1})$. The probabilities for one flagellum to be in the normal, curly-1, or semicoiled confirmation are then $P_{\mathrm{NORMAL}} = 1 - P_{\mathrm{CW}}$, $P_{\mathrm{CURLY}} = P_{\mathrm{CURLY|CW}} P_{\mathrm{CW}}$, and $P_{\mathrm{SEMI}} = 1 - P_{\mathrm{CURLY}} - P_{\mathrm{NORMAL}}$, respectively. For a cell with N flagella to be running, no flagella can be in the semicoiled and a minimum number of flagella, x, must be in the normal conformation to form a bundle. In the main text we assume $x = 2$ (the case $x = N - 2$ is considered in *SI Appendix*, Fig. S3). Accordingly, the steady-state probability to run is $P_{\mathrm{RUN}} = \sum_{j=x}^{N} P_j$, where $P_j = {}^N C_j P_{\mathrm{CURLY}}^{N-j} P_{\mathrm{NORMAL}}^{j}$ is the probability that j flagella are in the normal conformation and zero are in the semicoiled conformation. ${}^N C_j$ is the binomial coefficient. The rate of run termination is $k_T = k_- \langle j|\mathrm{RUN}\rangle$, where $\langle j|\mathrm{RUN}\rangle = \sum_{j=x}^{N} P_j j / P_{\mathrm{RUN}}$ is the average number of flagella in the normal conformation given that the cell is running. From these definitions, all other key dynamical properties of the conformation model in steady state (with $d \approx 0$) can be derived including the switching rate between runs and tumbles and the rate of resuming a run after a tumble event (*SI Appendix*).

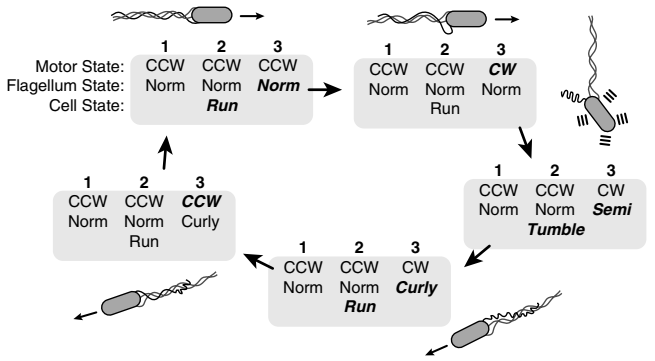

Fig. 1. Schematic diagram of a typical tumble event and the conformation model of multiple flagella. A switch to clockwise rotation of a flagellar motor induces a conformational change of the associated flagellum from a left-handed normal state to a right-handed semicoiled state after a short delay. This conformational change causes the cell to tumble. After a variable waiting time, the flagellum can adopt the more stable right-handed curly-1 conformation and wrap around the main flagellar bundle, which allows the cell to begin a new run. When the motor switches back to counterclockwise rotation, the flagellum readopts the normal conformation and the run persists. The conformation model tracks the rotational direction, flagellar conformation, and state of the cell according to these interaction rules over time.

Although this model neglects more complicated hydrodynamic effects and their possible feedback on motor switching (15–19) (see *Discussion*), it does effectively capture how a single motor switching to CW rotation generates a tumble, which is the primary mechanism by which runs may be cut short. Our model differs from previous studies (11) by considering flagellar conformations explicitly. It also differs from other previous works that ignore multiple flagella (13, 14, 27, 28), adopt a voting model in which a cell runs when a threshold number of motors are in CCW rotation (25, 26, 29), or represent the flagellar bundle state by using a distortion factor that grows with time spent in CW rotation (30).

Multiple Flagella Improve Detection of Fast Signals. We first assessed how the tumble bias and switching frequency between run-and-tumble states are affected by multiple flagella. Increasing the number of flagella moderately increased the tumble bias of the cell as a function of Y_p in the range of low to moderate CW bias of the individual motor ($Y_p < 3$ μM) (Fig. 2*A* and *SI Appendix*, Fig. S3 for the case $x = N - 2$) and increased the switching frequency between runs and tumbles (Fig. 2*B*). Additionally, at steady state, cells with multiple flagella switched from run to tumble at a higher rate than cells with a single flagellum but the same tumble bias (Fig. 2*C*), which was expected because any flagellum could induce a tumble. The rate of switching from a tumble to a run as a function of tumble bias increased similarly with the number of flagella (Fig. 2*D*). For Y_p between 2 and 3 μM, tumbles were often generated by a single flagellum that had sufficient time to switch to curly-1 and wrap around the main bundle before the corresponding motor switched back to CCW.

We then tested the effect of multiple flagella on a cell's response to step changes in Y_p by recording the response lag defined as the mean time after the step change to the start of the next run or tumble event. This metric is similar to that used to measure single cell response to steps in chemoattractant (6, 10, 31). We found that cells with multiple flagella generated a tumble more quickly in response to step increases in Y_p as compared to cells with a single flagellum (Fig. 2*E*) by as much as 0.5 s for Y_p increases of 0.4 μM. This result is in general agreement with experiments which exposed tethered (one flagellum) and free-swimming cells (multiple flagella) to step stimuli of repellant, which tends to increase Y_p (10). Multiple flagella also reduced the latency of response to small drops in Y_p; however, in this case the effect on cellular behavior is more marginal and difficult to

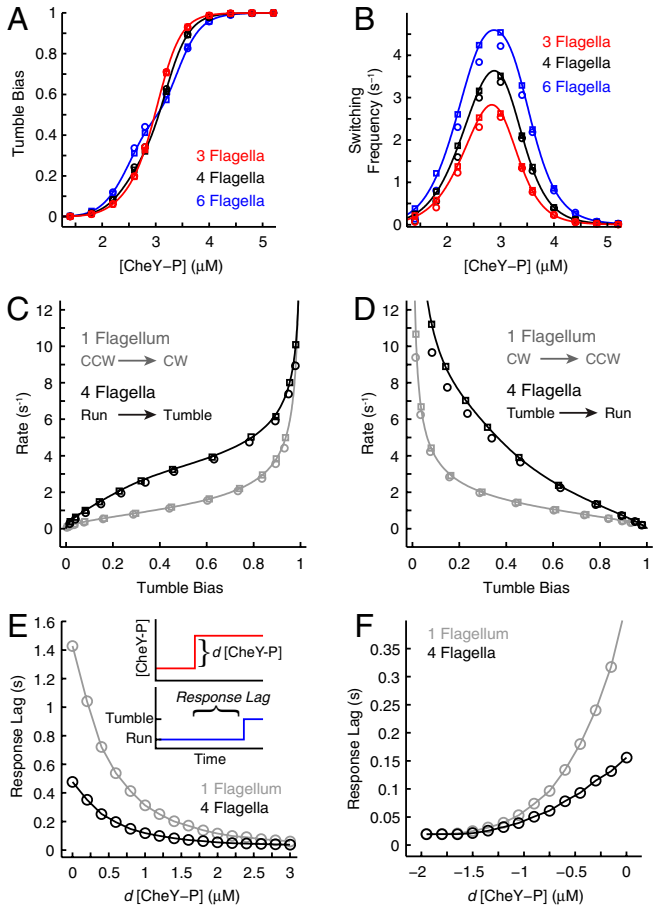

Fig. 2. Steady-state properties of the multiple flagella model. (*A*) Probability to be tumbling (tumble bias) and (*B*) rate of switching between run-and-tumble states as a function of Y_p. (*C*) Rate of switching from run to tumble for a cell with one (gray line) or four (black line) flagella. (*D*) The same as *C* but for the tumble to run transition. In *A–D*, solid lines are computed from the analytic model $P_{RUN} = (P_{CURLY} + P_{NORMAL})^N - (1 + N \cdot P_{NORMAL}/P_{CURLY})\, P_{CURLY}^N$ with $x = 2$. Circles are numerical simulations, and squares are numerical simulations where time delays are set to zero to match the analytic approximation. (*E*) Response lag to step increases in Y_p for cells with one (gray line) or four (black line) flagellar motors, computed as the mean time to switch from a run to a tumble after presentation of the stimulus as shown in the *Inset*. (*F*) The same as *E* but for a step decrease in Y_p. Initial values of Y_p in *C–D* were chosen so that the tumble bias of all cells was 0.23. Open circles are results of numerical simulations, and lines are to guide the eye.

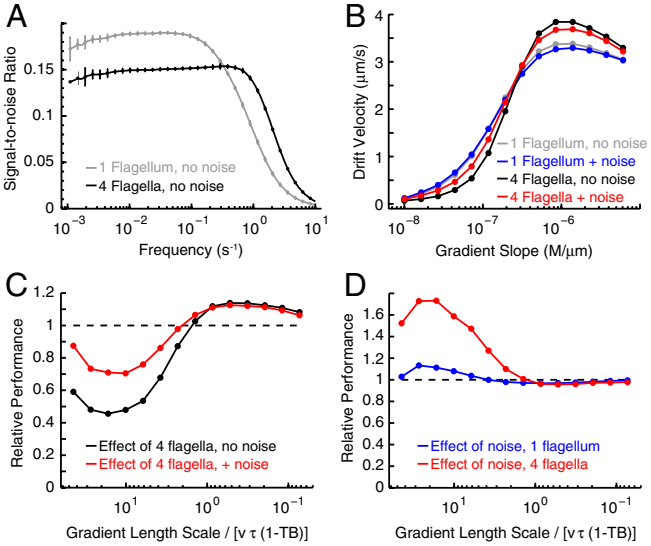

Fig. 3. Effect of multiple flagellar motors and signaling noise on signal transduction and chemotactic performance. (*A*) Frequency response to periodic stimuli in Y_p with an amplitude of 1 μM recorded for the output rotational state of a single motor and the run-and-tumble output of a cell with four motors. The SNR for each point was computed over 20 replicates of 60,000 s simulations. Error bars show the standard deviation over the 20 replicates. (*B*) Instantaneous drift velocity as a function of slope on linear gradients of methyl-aspartate measured at 1 min after the start of the simulation. Results shown for cells with a single flagellum in which the CCW or CW rotation is used as a proxy for runs and tumbles, respectively (gray line), cells with a single flagellar motor and noise of CV 0.15 (blue line), cells with four motors (black line), or cells with four motors and noise with CV 0.15 (red line). Cells begin adapted to the initial background concentration of 0.1 mM. Results were averaged over 18,000 cells for each population. All cells have tumble bias TB = 0.25, an adaptation time scale $\tau = 15$ s, and a run velocity $v = 20$ μm/s. (*C*) Relative effect of multiple motors on chemotactic performance: drift velocity of cells with multiple motors normalized by that of cells with a single motor for cases with (red line) and without (black line) signaling noise. (*D*) Relative effect of signaling noise on chemotactic performance: drift velocity of cells with signaling noise normalized by that of cells lacking signaling noise for the cases of single (blue line) and multiple (red line) motors. The length scale of the linear gradient is calculated as $L/(dL/dx)$ at the initial position of the cell where the ligand concentration is $L = 0.1$ mM.

observe (*SI Appendix*, Fig. S4) because of the small time scales involved (approximately 0.09 s for Y_p decreases of 0.4 μM) (Fig. 2*F*). Consistent with these results (*SI Appendix*, Fig. S4), experiments that exposed tethered and free-swimming cells to steps of attractant found little appreciable difference in the average response times (12). We note that the reduced latency of the response due to multiple flagella also depended on tumble bias and that for cells with a much higher tumble bias the effect should be more pronounced (*SI Appendix*, Fig. S5).

Next we investigated whether the faster response of the multiflagella system would enable detection of faster signals. We stimulated the multiple flagellar system with low amplitude sinusoidal signals in Y_p at varying frequencies and calculated the signal-to-noise ratio (SNR), defined as the integrated power at the signal frequency divided by the integrated background noise (*SI Appendix*, Fig. S10). We found that multiple flagella reduced the SNR for frequencies lower than 0.3 s^{-1} (time scales greater than 3.3 s) but improved detection of high-frequency signals compared to the rotational output of a single flagellum (Fig. 3*A*). This result is consistent with the faster response of multiple flagella to step changes in Y_p (Fig 2 *C–F*) but illustrates a trade-off in detecting lower-frequency signals.

Multiple Flagella Enhance Chemotactic Performance on Steep Gradients but Impair Chemotactic Performance on Shallow Gradients. Next we tested the implications of the enhanced detection of fast signals on chemotactic performance. We constructed a stochastic model of the chemotaxis signaling network adapted from recent, experimentally validated models (13, 25, 26, 32–35). As in many of these previous studies, the cooperative response of chemoreceptors was represented with a Monod-Wyman-Changeux (MWC) model (*Methods*). We also built an agent-based model of cell motion in 3D that accounted for rotational diffusion and directional persistence after tumbles (36) (*Methods*).

We simulated cells with either one or four flagellar motors over a wide range of linear gradients of the chemoattractant methyl-aspartate (Fig. 3*B*). The addition of multiple flagella increased the drift velocity of cells on steep gradients by up to 14% (Fig. 3*C*). Because cells with multiple flagella are able to tumble more rapidly in response to a stimulus drop (Fig. 2*F*), they are able to more quickly alter their heading when moving against the gradient. However, on shallow gradients, we found that the presence of multiple flagellar motors reduced the drift velocity by up

to 54% (Fig. 3*C*). Along shallow gradients, cells must move a longer distance to detect a change in attractant concentration. The higher tumbling rate of cells with multiple flagella is detrimental, because it prevents cells from sampling over large enough distances to make meaningful comparisons of attractant concentration. An increase in the number of flagellar motors thus introduced a trade-off in which response to steep gradients was improved at the expense of performance on shallow gradients.

How might a cell with multiple flagella cope with reduced performance on shallow gradients? We hypothesized that the reduced performance could be partially offset by considering fluctuations in the internal Y_p signal that could help coordinate motor switching, thus lengthening runs and improving detection of shallow gradients. Therefore we next investigated the role of signaling noise within the context of signal processing by multiple motors.

Signaling Noise Coordinates the Switching Statistics of Multiple Flagellar Motors. By monitoring multiple motors in a single cell (29), Berg and colleagues discovered that the rotational biases of adjacent flagellar motors were significantly correlated over a time scale of approximately 10 s (Fig. 4*A*). Recently, correlations between the switching events of two adjacent motors were documented on a subsecond time scale (37) and found to depend on the precise location of the motors in relation to the receptor cluster. Although motor coordination over fast time scales may result from the localization of CheA and CheZ coupled to the fast dynamics of CheY phosphorylation and diffusion (37), the much slower coordinated variations observed in the earlier study were unexpected, because the cells were adapted to their environment without any apparent time-varying stimuli (29).

Recent experimental and theoretical work, however, demonstrated that individual flagellar motors in nonstimulated *E. coli* cells can exhibit slow fluctuations with time scales on the order of 10–30 s originating from the adaptation reactions (11, 13, 31). We reasoned that the long correlation time of single motors and coordination of multiple motors both arise from slow fluctuations in the adaptation kinetics. To test this hypothesis, we simulated pairs of flagellar motors with Gaussian-distributed fluctuations in Y_p (*Methods*). We found that Y_p fluctuations with 12-s time correlation and coefficient of variation (CV) of 0.10 reproduced the coordinated response of adjacent motors (29) (Fig. 4*A*). For similar values of the correlation time (between 5 and 35 s) and noise strength ($0.05 \leq \mathrm{CV} \leq 0.2$), the same model with all other parameters held constant reproduced the fluctuations measured from single motors in wild-type cells (11, 31). For example, we accounted for the power spectrum of the wild-type cell reported in ref. 11 with simulations of a single motor subject to fluctuations in Y_p with a correlation time of 30 s and a CV of 0.15 (*SI Appendix*, Fig. S6). Thus, the early experiments on adjacent motors (29) add an independent verification of the high degree of signaling noise in the bacterial chemotaxis pathway.

Increasing the magnitude of the input noise increased the correlation coefficient for all positive values of the correlation time as measured by the linear (Pearson) correlation coefficient between pairs of motor output (Fig. 4*B*). The magnitude of motor coordination also increased with the time scale of the noise over the entire range tested (*SI Appendix*, Fig. S7), although the dependence was strongest in the region up to approximately 1 s (indicated in Fig. 4*B* with a dashed line), which is the approximate time scale of motor switching. For reference, in Fig. 4*B* we indicate the time scale and CV of the noise corresponding to the cell in Fig. 4*A* (29) and the wild-type cell in *SI Appendix*, Fig. S6 (11).

Signaling Noise Generates Long-Tailed Run Length Distributions to Enhance Exploration. The finding that slow fluctuations in Y_p can generate a long tail in the CCW interval distribution of a single motor (11, 14, 24) has led to the hypothesis that slow fluctuations may enhance the exploration of a cell by generating a movement pattern with characteristics of a Lévy walk (11, 13, 14, 27, 37). These studies assumed that long CCW intervals of single motors translate directly to longer runs. However, runs may be cut short by the CW rotation of a single flagellum (2, 3). We sought to establish if the slow spontaneous fluctuations arising within the adaptation mechanism are sufficient to produce a long tail in the run length distribution of a multiflagellated cell and then investigated how this noise influences chemotactic performance.

We found that for time scales and magnitude of noise similar to those measured experimentally (11, 29, 31), long tails in CCW event duration of single motors generated long tails in the run length distribution (*SI Appendix*, Fig. S9). Generation of long runs required not only slow fluctuations in Y_p but also the coordination of motors. When the motors were uncoordinated with independent but equally noisy Y_p input with the same mean, we observed that long runs were interrupted, which created a nearly exponential run length distribution (*SI Appendix*, Fig. S9) even though the individual motors still exhibited long intervals of CCW rotation.

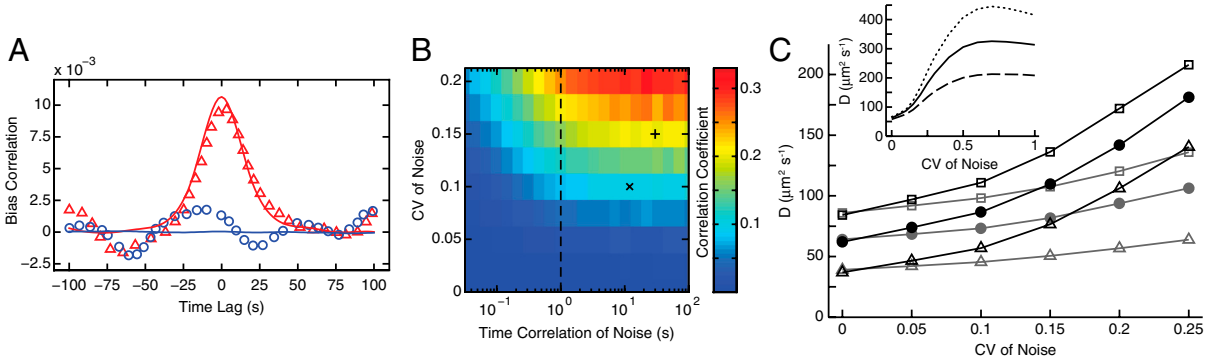

Fig. 4. Signaling noise coordinates the switching statistics of multiple flagellar motors and enhances exploration. (*A*) Bias correlation of adjacent flagellar motors in a single filamentous cell (red triangles) as compared to motors from separate cells (blue circles). Experimental data are from ref. 29. Simulations of two flagellar motors on the same cell (red line) with input noise in Y_p exhibiting 12-s time correlations and a CV of 0.1 and without noisy input (blue line). (*B*) Coordination of motors computed as the linear (Pearson) correlation coefficient. The CV and time correlation of noise predicted for the filamentous cell in *A* and the wild-type cell from ref. 11 are indicated with × and +, respectively. The dashed line indicates the approximate time scale of motor switching (1 s). (*D*) The effective diffusion coefficient *D* for coordinated (black) and uncoordinated (gray) motors for populations of cells with either three (squares), four (circles), or six (triangle) flagella per cell. (*Inset*) Diffusion coefficient as a function of signaling noise for cells with four flagellar motors and a rotational diffusion constant of 0.031 (dotted line), 0.062 (solid line), or 0.124 rad^2/s (dashed line). Results were averaged over 4,000 cells for each population. All cells have a mean tumble bias of 0.25.

We then quantified the degree to which noise, motor coordination, and the number of flagella affect searching in the absence of stimuli. We simulated the run-and-tumble motion of bacteria with either coordinated or uncoordinated motors over a range of signaling noise strengths and calculated the effective diffusion coefficient (Fig. 4*C*). The diffusion coefficient of cells increased with the CV of the noise. At the same noise level, cells with coordinated motors diffused significantly farther than cells with uncoordinated motors. Increasing the number of motors decreased the space explored by a cell, because long runs were more likely to be interrupted by a single motor switching to CW rotation. This effect could be partially mitigated by increasing the magnitude of signaling noise. The effective diffusion coefficient eventually saturated at a high magnitude of noise (CV = 0.6) (Fig. 4*C*, *Inset*). The maximal effective diffusion coefficient depended on both the time scale of the signaling noise, which imposed an upper limit on the duration of a run (*SI Appendix*, Fig. S12), and the rotational diffusion, which limited the contribution of the longest runs to increased diffusion (Fig. 4*C*, *Inset*). These limits were reached only with a magnitude of noise much higher than was observed in wild-type cells (11, 31). Therefore, over the physiological range of noise magnitudes, our model predicts that added signaling noise will always enhance exploration of cells.

The Long Tail of the Run Length Distribution Enhances Sensitivity to Shallow Gradients. How does signaling noise influence signal transduction and chemotactic performance? Surprisingly, although the presence of noise reduced the SNR across all frequencies (*SI Appendix*, Fig. S11), noise improved chemotactic performance on shallow gradients for cells with either single or multiple flagella (Fig. 3 *B* and *D*). This result highlights an interesting relationship between the run length and the local length scale of the gradient. On very shallow gradients, the length scale of the gradient becomes much longer than cell runs, which makes it difficult for the cell to detect the gradient. The occasional long runs generated by signaling noise improve performance on shallow gradients (Fig. 3*B*) by enabling cells to make comparisons of ligand concentration over longer distances. In the case of a single flagellum, this effect increased drift velocity by up to 13% (Fig. 3*D*). For a cell with multiple flagella, the signaling noise had the additional effect of coordinating the switching statistics of multiple motors, which allowed the longer CCW rotation events in single motors to generate long runs. The combined effects of the occasional long CCW intervals and coordination significantly enhanced performance on shallow gradients by up to 73% (Fig. 3*D*). This advantage disappeared when the long tail in the run length distribution of the noisy cells was eliminated by artificially uncoordinating the motors (*SI Appendix*, Fig S15). Thus, although the presence of multiple flagella reduces performance on shallow gradients, signaling noise partially compensates for this reduction (Fig. 3*C*) while introducing only a modest penalty on steep gradients.

Discussion

Bacterial chemotaxis provides a model system to study the effect of multiple, independent stochastic actuators on signal transduction and cellular behavior. The inclusion of multiple motors improved the detection of fast signals and decreased the lag time in response to negative stimulus, which leads to improved performance on steep attractant gradients. However, the inclusion of multiple motors introduced drawbacks as well, because independently fluctuating actuators are much less likely to produce a sustained response. For bacterial chemotaxis, this incoherence resulted in shortened run lengths that reduce the ability of the cells to explore their environment and track shallow gradients.

Signaling noise provided a means to coordinate the output of multiple independent actuators. In the chemotaxis system, signaling noise has already been shown to extend the CCW intervals of a single motor (11, 13, 14, 24, 37) and has been hypothesized to have the same effect on run length. Long tails in the run length distribution are known to enhance exploration capabilities of random walkers by enabling them to search on multiple scales (11, 38, 39). Here we found that, in addition to enhancing exploration, the occasional long runs enhance the ability of a cell to track shallow gradients by enabling it to sample the gradient over appropriately long length scales. In the case of multiple motors, signaling noise enabled the motors to generate long CCW events in a coordinated manner, which leads to sustained runs. This effect strongly reduces the negative impact of multiple flagella on the performance in shallow gradients with only a slight cost on steep gradients. Our analysis suggests that the combination of multiple motors and signaling noise enables *E. coli* to perform effective chemotaxis across a range of environments.

These results highlight the need to study the effects of fluctuations within a behavioral context, because a reduction in signal transduction fidelity did not necessarily translate into diminished behavioral performance. Intracellular signaling noise degraded SNR across all frequencies yet still benefited chemotactic performance. In the chemotaxis system, noise in the output feeds back into the input. By lengthening runs, noise functioned to alter the pattern with which the cell sampled its environment. This example differs from instances of noise-enhanced behavior in which noise directly improves signal processing fidelity, such as stochastic resonance (40).

Our work suggests further directions for theory and experiment. In future studies, it may be instructive to extend existing models of the motor (19, 20, 22, 41, 42) to incorporate more details about the effects of flagellar hydrodynamics (15–17) and mechanical feedback on the switching rates of the motors (18, 19, 43, 44). Because there is some indication that the torque-speed relationship of the flagellar motor depends on Y_p (45), proper calibration and extension of current models of the motor would require expanding existing measurements of the torque-speed-switching rate relations (18, 19, 43, 44) to include varying levels of Y_p. The present study required repeated simulation of large cellular populations. Therefore we used a coarse-grained model that captures Berg and colleagues' essential observations of flagellar conformations, as well as single cell data on motor switching, while still enabling rapid simulations. Predictions from our model concerning motor count and gradient tracking could be tested by experiments in which the motion of individual bacteria is tracked (36) and the number of flagella subsequently counted.

Our results illustrate how the action of multiple, independent components can be integrated by signaling systems to form a coherent cellular response. The presence of multiple actuators allows a response time shorter than the time scale of the stochastic switching of a single actuator and, therefore, increases the bandwidth of the system at high frequencies. On the other hand, independent fluctuations of the actuators have the potential to create an incoherent output. Upstream low-frequency noise can help overcome this challenge by coordinating actuator responses. In the case of bacterial chemotaxis, the steep sensitivity of the flagellar motor to changes in Y_p is consistent with this model of performance enhancement through coordination by time-correlated noise. If the motor response were less steep, spontaneous fluctuations in Y_p would be less likely to induce near-simultaneous switches in multiple motors, which would reduce the level of coordination. Similarly important was the relatively fast switching rate of the motor, which ensured that multiple motors were likely to switch within the correlation time scale of the signaling noise. Stochastic actuators in other systems that show coordinated response may well share these characteristics. For example, recent work has shown that expression of genes with different promoter strengths can be coordinated by noisy bursts of nuclear

localization of transcription factors, which allows signals to be encoded in the frequency of bursts (46, 47). We anticipate that coordination of independent downstream actuators by a common noisy input might be a feature implemented by other biological systems as well, such as membrane transport proteins, membrane channels, and molecular motors.

Methods

Model of Chemotaxis Signaling and Adaptation. Recent models (13, 25, 32, 33, 35) were adapted to simulate the chemotactic response to methyl-aspartate. Chemoreceptor complexes were represented with a MWC model (48) in which receptor homodimers assemble into fully cooperative signaling teams that switch rapidly between active (on) and inactive (off) conformations. The free energy difference F in units of k_BT between the active and inactive states of the complex is

$$F = \varepsilon_0 + \varepsilon_1 m + \sum_r \log\left(\frac{1+[L]/K_r^{\text{off}}}{1+[L]/K_r^{\text{on}}}\right)^{n_r} \quad [3]$$

in which m is the total methylation level of the complex, r indicates the receptor species (Tar or Tsr), and K_r^{off} and K_r^{on} are binding constants between methyl-aspartate and the two dimer conformations. The probability of the complex to be in the active state is $A = 1/(1+e^F)$. We assume a linear relationship $Y_p(t) = \alpha A(t)$ between receptor activity and Y_p (25). Parameter values were $K_{\text{TAR}}^{\text{off}} = 0.02$ mM, $K_{\text{TAR}}^{\text{on}} = 0.4$ mM, $K_{\text{TSR}}^{\text{off}} = 100$ mM, $K_{\text{TSR}}^{\text{on}} = 10^6$ mM (33, 35), $\epsilon_0 = 1.0$, $\epsilon_1 = -0.45$, $\alpha = 6$ μM, $n_{\text{Tar}} = 6$, and $n_{\text{Tsr}} = 13$.

Methylation kinetics were modeled by the Ornstein-Uhlenbeck (OU) process (49):

$$\frac{dm}{dt} = -\frac{1}{\tau}[m(t) - \bar{m}(L)] + \sigma_m\sqrt{2/\tau}\Gamma(t), \quad [4]$$

where τ is the relaxation time, $\sigma_m{}^2$ is the variance of fluctuations in the methylation level, $\Gamma(t)$ is a normally distributed random process with a zero mean and unit variance, and $\bar{m}$ is the methylation level needed to achieve the specified steady-state activity given L. For simulations not requiring the full signaling system, fluctuations in Y_p were modeled by the OU process $dY_p/dt = -(Y_p - \bar{Y}_p)/\tau + \sigma_y\sqrt{2/\tau}\Gamma(t)$ in which $\bar{Y}_p$ and σ_y^2 are the mean and variance of Y_p, respectively.

Cell Movement in 3D Environments. Simulated bacteria have a constant run speed of 20 μm/s and, unless otherwise stated, a rotational diffusion constant of 0.062 rad^2/s (14, 26, 36, 50). As in past studies (14, 26), it is assumed that tumbling cells are stationary. After tumbles, cells are reoriented in a new direction that is randomly sampled from a gamma distribution with scale parameter 18.32 and shape parameter 4 to match the experimentally observed distribution of new run angles (14, 36).

Implementation and Simulation. Models were implemented and numerically simulated with custom Matlab and C++ code that utilizes some functionality of NFsim (23).

ACKNOWLEDGMENTS. We thank G. Jentsch for help with software development and Y. Dufour and N. Frankel for helpful discussions. Simulations were performed at the Yale University High Performance Computing Center. This work was supported by the National Science Foundation (CCF-0829836) and the James S. McDonnell Foundation.

1. Berg HC (2000) Motile behavior of bacteria. *Phys Today* 53:24–29.
2. Darnton NC, Turner L, Rojevsky S, Berg HC (2007) On torque and tumbling in swimming Escherichia coli. *J Bacteriol* 189:1756–1764.
3. Turner L, Ryu WS, Berg HC (2000) Real-time imaging of fluorescent flagellar filaments. *J Bacteriol* 182:2793–2801.
4. Wadhams GH, Armitage JP (2004) Making sense of it all: Bacterial chemotaxis. *Nat Rev Mol Cell Biol* 5:1024–1037.
5. Block SM, Segall JE, Berg HC (1982) Impulse responses in bacterial chemotaxis. *Cell* 31:215–226.
6. Segall JE, Manson MD, Berg HC (1982) Signal processing times in bacterial chemotaxis. *Nature* 296:855–857.
7. Fahrner KA (1995) Studies of bacterial flagellar motors and filaments. PhD thesis (Harvard Univ Press, Cambridge, MA).
8. Cluzel P, Surette M, Leibler S (2000) An ultrasensitive bacterial motor revealed by monitoring signaling proteins in single cells. *Science* 287:1652–1655.
9. Sourjik V, Berg HC (2004) Functional interactions between receptors in bacterial chemotaxis. *Nature* 428:437–441.
10. Khan S, Jain S, Reid GP, Trentham DR (2004) The fast tumble signal in bacterial chemotaxis. *Biophys J* 86:4049–4058.
11. Korobkova E, Emonet T, Vilar JMG, Shimizu TS, Cluzel P (2004) From molecular noise to behavioural variability in a single bacterium. *Nature* 428:574–578.
12. Jasuja R, Keyoung J, Reid GP, Trentham DR, Khan S (1999) Chemotactic responses of Escherichia coli to small jumps of photoreleased L-aspartate. *Biophys J* 76:1706–1719.
13. Emonet T, Cluzel P (2008) Relationship between cellular response and behavioral variability in bacterial chemotaxis. *Proc Natl Acad Sci USA* 105:3304–3309.
14. Emonet T, Macal CM, North MJ, Wickersham CE, Cluzel P (2005) AgentCell: A digital single-cell assay for bacterial chemotaxis. *Bioinformatics* 21:2714–2721.
15. Flores H, Lobaton E, Méndez-Diez S, Tlupova S, Cortez R (2005) A study of bacterial flagellar bundling. *Bull Math Biol* 67:137–168.
16. Kim M, Bird JC, Van Parys AJ, Breuer KS, Powers TR (2003) A macroscopic scale model of bacterial flagellar bundling. *Proc Natl Acad Sci USA* 100:15481–15485.
17. Lauga E, Powers TR (2009) The hydrodynamics of swimming microorganisms. *Rep Prog Phys* 72:096601.
18. Fahrner KA, Ryu WS, Berg HC (2003) Biomechanics: Bacterial flagellar switching under load. *Nature* 423:938.
19. Yuan J, Fahrner KA, Berg HC (2009) Switching of the bacterial flagellar motor near zero load. *J Mol Biol* 390:394–400.
20. Van Albada SB, Tänase-Nicola S, Ten Wolde PR (2009) The switching dynamics of the bacterial flagellar motor. *Mol Syst Biol* 5:316.
21. Tu Y (2008) The nonequilibrium mechanism for ultrasensitivity in a biological switch: Sensing by Maxwell's demons. *Proc Natl Acad Sci USA* 105:11737–11741.
22. Bai F, et al. (2010) Conformational spread as a mechanism for cooperativity in the bacterial flagellar switch. *Science* 327:685–689.
23. Sneddon MW, Faeder JR, Emonet T (2011) Efficient modeling, simulation and coarse-graining of biological complexity with NFsim. *Nat Methods* 8:177–183.
24. Tu Y, Grinstein G (2005) How white noise generates power-law switching in bacterial flagellar motors. *Phys Rev Lett* 94:208101.
25. Jiang L, Ouyang Q, Tu Y (2010) Quantitative modeling of Escherichia coli chemotactic motion in environments varying in space and time. *PLoS Comput Biol* 6:e1000735.
26. Vladimirov N, Løvdok L, Lebiedz D, Sourjik V (2008) Dependence of bacterial chemotaxis on gradient shape and adaptation rate. *PLoS Comput Biol* 4:e1000242.
27. Matthäus F, Jagodic M, Dobnikar J (2009) E. coli superdiffusion and chemotaxis-search strategy, precision, and motility. *Biophys J* 97:946–957.
28. Kalinin YV, Jiang L, Tu Y, Wu M (2009) Logarithmic sensing in Escherichia coli bacterial chemotaxis. *Biophys J* 96:2439–2448.
29. Ishihara A, Segall JE, Block SM, Berg HC (1983) Coordination of flagella on filamentous cells of Escherichia coli. *J Bacteriol* 155:228–237.
30. Vladimirov N, Lebiedz D, Sourjik V (2010) Predicted auxiliary navigation mechanism of peritrichously flagellated chemotactic bacteria. *PLoS Comput Biol* 6:e1000717.
31. Park H, et al. (2010) Interdependence of behavioural variability and response to small stimuli in bacteria. *Nature* 468:819–823.
32. Mello BA, Tu Y (2005) An allosteric model for heterogeneous receptor complexes: Understanding bacterial chemotaxis responses to multiple stimuli. *Proc Natl Acad Sci USA* 102:17354–17359.
33. Endres RG, Wingreen NS (2006) Precise adaptation in bacterial chemotaxis through "assistance neighborhoods". *Proc Natl Acad Sci USA* 103:13040–13044.
34. Keymer JE, Endres RG, Skoge M, Meir Y, Wingreen NS (2006) Chemosensing in Escherichia coli: Two regimes of two-state receptors. *Proc Natl Acad Sci USA* 103:1786–1791.
35. Hansen CH, Endres RG, Wingreen NS (2008) Chemotaxis in Escherichia coli: A molecular model for robust precise adaptation. *PLoS Comput Biol* 4:e1.
36. Berg HC, Brown DA (1972) Chemotaxis in Escherichia coli analysed by three-dimensional tracking. *Nature* 239:500–504.
37. Matthäus F, Mommer MS, Curk T, Dobnikar J (2011) On the origin and characteristics of noise-induced Lévy walks of E. coli. *PLoS One* 6:e18623.
38. Viswanathan GM, et al. (1999) Optimizing the success of random searches. *Nature* 401:911–914.
39. Edwards AM, et al. (2007) Revisiting Levy flight search patterns of wandering albatrosses, bumblebees and deer. *Nature* 449:1044–1048.
40. Gammaitoni L, Hänggi P, Jung P, Marchesoni F (1998) Stochastic resonance. *Rev Mod Phys* 70:223–223.
41. Duke TAJ, Le Novere N, Bray D (2001) Conformational spread in a ring of proteins: A stochastic approach to allostery1. *J Mol Biol* 308:541–553.
42. Meacci G, Lan G, Tu Y (2011) Dynamics of the bacterial flagellar motor: The effects of stator compliance, back steps, temperature, and rotational asymmetry. *Biophys J* 100:1986–1995.
43. Chen X, Berg HC (2000) Torque-speed relationship of the flagellar rotary motor of Escherichia coli. *Biophys J* 78:1036–1041.
44. Yuan J, Berg HC (2008) Resurrection of the flagellar rotary motor near zero load. *Proc Natl Acad Sci USA* 105:1182–1185.
45. Yuan J, Fahrner KA, Turner L, Berg HC (2010) Asymmetry in the clockwise and counterclockwise rotation of the bacterial flagellar motor. *Proc Natl Acad Sci USA* 107:12846–12849.
46. Cai L, Dalal CK, Elowitz MB (2008) Frequency-modulated nuclear localization bursts coordinate gene regulation. *Nature* 455:485–490.
47. Eldar A, Elowitz MB (2010) Functional roles for noise in genetic circuits. *Nature* 467:167–173.
48. Monod J, Wyman J, Changeux J-P (1965) On the nature of allosteric transitions: A plausible model. *J Mol Biol* 12:88–118.
49. Gillespie DT (1996) The mathematics of Brownian motion and Johnson noise. *Am J Phys* 64:225–240.
50. Berg HC (1993) *Random Walks in Biology* (Princeton Univ Press, Princeton, NJ).